Cell Reports

Article

The 9-1-1 Complex Controls Mre11 Nuclease and Checkpoint Activation during Short-Range Resection of DNA Double-Strand Breaks

Graphical Abstract

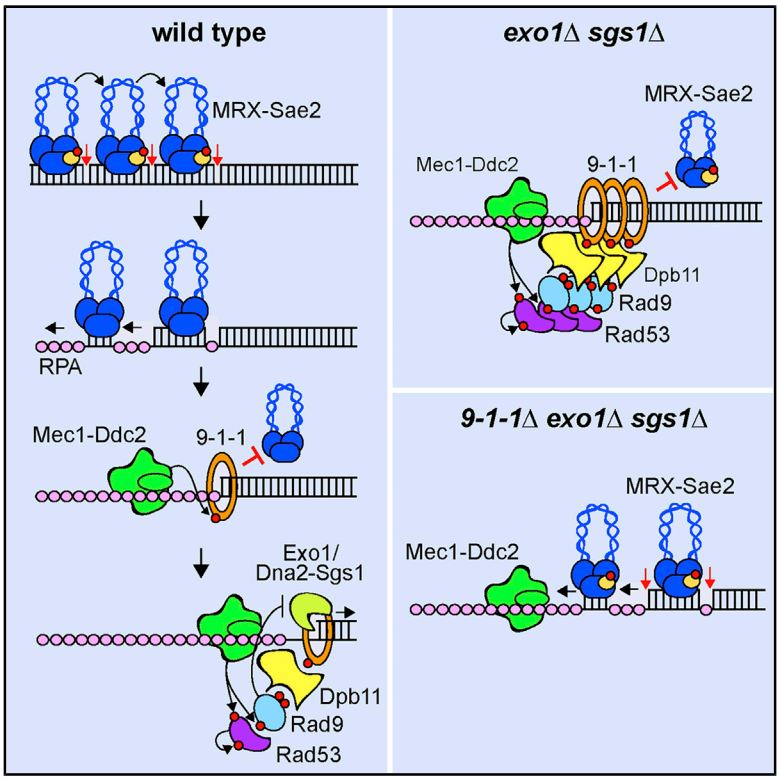

Highlights

- The 9-1-1 complex induces a checkpoint in the absence of both Exo1 and Sgs1
- Checkpoint activation decreases DNA damage resistance of *exo1Δ sgs1Δ* cells
- The 9-1-1 complex negatively regulates short-range resection
- The 9-1-1 complex restricts Mre11 nuclease close to the double-strand break end

Authors

Elisa Gobbini, Erika Casari, Chiara Vittoria Colombo, Diego Bonetti, Maria Pia Longhese

Correspondence

mariapia.longhese@unimib.it

In Brief

Resection of DNA double-strand breaks is a two-step process that relies on short and long-range nucleases. Gobbini et al. show that the 9-1-1 complex plays a dual function during short-range resection, promoting checkpoint activation by recruiting Rad9 at damaged sites and negatively regulating short-range resection in a Rad9-independent manner by restricting Mre11 nuclease.

Gobbini et al., 2020, Cell Reports *33*, 108287
October 20, 2020
https://doi.org/10.1016/j.celrep.2020.108287

CellPress

Cell Reports

CellPress
OPEN ACCESS

Article

The 9-1-1 Complex Controls Mre11 Nuclease and Checkpoint Activation during Short-Range Resection of DNA Double-Strand Breaks

Elisa Gobbini,[1] Erika Casari,[1] Chiara Vittoria Colombo,[1] Diego Bonetti,[1] and Maria Pia Longhese[1,2,*]
[1]Dipartimento di Biotecnologie e Bioscienze, Università degli Studi di Milano-Bicocca, Milano 20126, Italy
[2]Lead Contact
*Correspondence: mariapia.longhese@unimib.it
https://doi.org/10.1016/j.celrep.2020.108287

SUMMARY

Homologous recombination is initiated by nucleolytic degradation (resection) of DNA double-strand breaks (DSBs). DSB resection is a two-step process in which an initial short-range step is catalyzed by the Mre11-Rad50-Xrs2 (MRX) complex and limited to the vicinity of the DSB end. Then the two long-range resection Exo1 and Dna2-Sgs1 nucleases extend the resected DNA tracts. How short-range resection is regulated and contributes to checkpoint activation remains to be determined. Here, we show that abrogation of long-range resection induces a checkpoint response that decreases DNA damage resistance. This checkpoint depends on the 9-1-1 complex, which recruits Dpb11 and Rad9 at damaged DNA. Furthermore, the 9-1-1 complex, independently of Dpb11 and Rad9, restricts short-range resection by negatively regulating Mre11 nuclease. We propose that 9-1-1, which is loaded at the leading edge of resection, plays a key function in regulating Mre11 nuclease and checkpoint activation once DSB resection is initiated.

INTRODUCTION

DNA double-strand breaks (DSBs) can be repaired by homologous recombination (HR), which uses intact homologous duplex DNA as a template to restore the genetic information lost at the break site (Kowalczykowski, 2015; Mehta and Haber, 2014). The first step of HR is the degradation of the 5′-terminated DNA strands on either side of the DSB to generate 3′ ended single-stranded DNA (ssDNA) tails through a process termed DNA end resection (Bonetti et al., 2018).

In both yeast and mammals, DNA end resection can be a two-step process that involves sequential engagement of short-range and long-range nucleases (Bonetti et al., 2018). In short-range resection, the endonuclease activity of the Mre11-Rad50-Xrs2/NBS1 (MRX/N) complex, aided by the Sae2 protein (CtIP in mammals), cleaves the 5′-terminated DNA strand of the DSB end (Cannavo and Cejka, 2014), followed by the Mre11 3′-5′ exonuclease that proceeds back toward the DSB end (Mimitou and Symington, 2008; Zhu et al., 2008; Garcia et al., 2011; Shibata et al., 2014; Reginato et al., 2017; Wang et al., 2017). Although this resection is limited to the vicinity of the DNA end, it has the capacity to process DNA ends with secondary DNA structures and bound protein blocks. The second phase is a long-range resection, which resects nucleotides in the 5′-3′ direction away from the DSB ends and is carried out by either Exo1 or Dna2 in conjunction with the helicase Sgs1 (WRN or BLM in mammals) (Mimitou and Symington, 2008; Zhu et al., 2008; Cejka et al., 2010; Nicolette et al., 2010; Niu et al., 2010; Nimonkar et al., 2011; Cannavo et al., 2013; Reginato et al., 2017; Wang et al., 2017).

The resection activity of Sgs1-Dna2 is inhibited by the *S. cerevisiae* Rad9 protein (53BP1 in mammals) (Lazzaro et al., 2008; Clerici et al., 2014; Bonetti et al., 2015; Ferrari et al., 2015), whose association to chromatin involves multiple pathways. Rad9 interacts with histone H3 in its K79-methylated form (H3-K79me) (Wysocki et al., 2005; Grenon et al., 2007), a chromatin modification that is introduced by the methyltransferase Dot1 (Giannattasio et al., 2005; Toh et al., 2006). Rad9 can also bind to histone H2A that has been phosphorylated at Ser 129 (γH2A) by the checkpoint kinases Mec1 (ATR in mammals) and Tel1 (ATM in mammals) (Downs et al., 2000; Shroff et al., 2004; Toh et al., 2006; Hammet et al., 2007). Finally, phosphorylation of Ser 462 and Thr 474 residues of Rad9 by cyclin-dependent kinase (Cdk1) leads to Rad9 interaction with the multi-BRCT domain protein Dpb11 (TopBP1 in mammals) (Granata et al., 2010; Pfander and Diffley, 2011; Cussiol et al., 2015).

Dpb11 in turn is recruited to DSBs by the evolutionarily conserved Ddc1-Mec3-Rad17 (Rad9-Hus1-Rad1 in mammals) complex (hereafter referred to as 9-1-1), which is a ring-shaped heterotrimer that is loaded at ssDNA-double-stranded DNA (dsDNA) junctions by the clamp loader Rad24 (RAD17 in mammals)-replication factor C subunits 2–5 (Rfc2–Rfc5) (Majka et al., 2006; Navadgi-Patil and Burgers, 2009). In budding yeast, the interaction between Dpb11 and 9-1-1 requires phosphorylation of Ddc1 Thr 602 and this phospho-dependent Dpb11-Ddc1 binding is conserved in mammals (Delacroix et al., 2007; Puddu et al., 2008; Navadgi-Patil and Burgers, 2009). By promoting the association of Rad9 at DSBs, the 9-1-1 complex counteracts the resection activity of the long-range resection nucleases Exo1

and Dna2 (Ngo and Lydall, 2015). Furthermore, Rad9, Dpb11 and 9-1-1 are required to activate the checkpoint kinase Mec1 (ATR in humans) (Mordes et al., 2008; Navadgi-Patil and Burgers, 2008, 2009), which senses the presence of ssDNA via interaction with replication protein A (RPA) (Zou and Elledge, 2003) and activates the downstream effector kinases Rad53 (CHK2 in mammals) and Chk1 (Villa et al., 2016).

Although much progress has been made in understanding the structural and functional activities of the MRX complex, how its nuclease activity is controlled remains to be determined. Furthermore, the physiological relevance of the long-range resection is not obvious, because although *exo1Δ sgs1Δ* budding yeast cells suffer sensitivity to DNA-damaging agents, the 100–300 nt of ssDNA generated by MRX-Sae2 cleavage events are sufficient for meiotic recombination and result only in a moderate decrease of ectopic recombination in vegetative growing *exo1Δ sgs1Δ* cells (Gravel et al., 2008; Zhu et al., 2008; Chung et al., 2010; Zakharyevich et al., 2010; Keelagher et al., 2011; Westmoreland and Resnick, 2016; Guo et al., 2017).

Here, we show that failure of 9-1-1 to recruit Dpb11 and Rad9 at damaged sites partially restores DNA damage resistance of *exo1Δ sgs1Δ* cells by decreasing Rad53 activation. Furthermore, the lack of 9-1-1 extends DSB resection in *exo1Δ sgs1Δ* cells in a manner that depends on Mre11 nuclease activity, but not on 9-1-1 function in recruiting Dpb11 and Rad9 to DSBs. Altogether, these data lead to a model whereby 9-1-1 plays a dual function during short-range resection, promoting checkpoint activation by recruiting Rad9 at damaged sites and negatively regulating MRX nuclease.

RESULTS

Screen for Suppressors of the DNA Damage Sensitivity of *exo1Δ sgs1Δ* Cells

Budding yeast cells lacking both Exo1 and Sgs1 can generate only short 3′ ended ssDNA tails resulting from MRX-Sae2-dependent cleavage events (Zhu et al., 2008; Mimitou and Symington, 2008; Guo et al., 2017). These cells show decreased viability even in the absence of DNA lesions. Moreover, they are hypersensitive both to the topoisomerase poison camptothecin (CPT), which leads to DSBs by stabilizing DNA topoisomerase I cleavage complexes, and to the ionizing-radiation-mimetic compound phleomycin (phleo). To identify mechanisms responsible for the DNA damage hypersensitivity of *exo1Δ sgs1Δ* cells, we searched for extragenic mutations that suppress their CPT and/or phleomycin sensitivity. CPT- and/or phleomycin-resistant *exo1Δ sgs1Δ* clones were crossed to each other and to the wild-type strain to identify, by tetrad analysis, 20 single-gene suppressor mutants that fell into eight distinct allelism groups. Genome sequencing of two non-allelic suppressor clones identified a *RAD24* single base-pair substitution, which introduces a STOP codon in place of Asp 334 (*rad24-E334**), and a *DPB11* single base-pair substitution, causing the replacement of Leu 410 residue with Phe (*dpb11-L410F*) (Figure 1A). The identity of the genes that are mutated in the remaining suppressor clones remains to be determined. As shown in Figure 1A, both *rad24-E334** and *dpb11-L410F* alleles partially suppressed the hypersensitivity to CPT and phleomycin of *exo1Δ sgs1Δ* cells. Suppression by the *rad24-E334** allele is likely due to loss of Rad24 function, as *RAD24* deletion suppressed the DNA damage sensitivity of *exo1Δ sgs1Δ* cells (Figure 1A). This test could not be performed for Dpb11 that is essential for cell viability.

The Lack of 9-1-1-Mediated Recruitment of Dpb11 Suppresses the DNA Damage Sensitivity of *exo1Δ sgs1Δ* Cells

Rad24 is part of the Rad24-RFC clamp loader, which loads the 9-1-1 complex to the ssDNA-dsDNA junctions at DNA lesions (Majka et al., 2006; Navadgi-Patil and Burgers, 2009). Once loaded onto DNA, the 9-1-1 clamp recruits Dpb11 to sites of DNA damage via interaction with Ddc1 (Wang and Elledge, 2002; Puddu et al., 2008; Pfander and Diffley, 2011) (Figure 1B). The interaction between Dpb11 and 9-1-1 requires phosphorylation by Mec1 of Thr 602 of Ddc1, which is then recognized by the BRCT3 and BRCT4 domains of Dpb11 (aa 276–600) (Puddu et al., 2008). As the *dpb11-L410P* mutation is located in the BRCT domain that mediates the interaction between Dpb11 and 9-1-1 (Pfander and Diffley, 2011), we asked whether 9-1-1 failure to recruit Dpb11 to damage sites was responsible for the suppression of *exo1Δ sgs1Δ* cells. The *ddc1-T602A* allele, which specifically abrogates 9-1-1 binding to Dpb11, partially suppressed the DNA damage sensitivity of *exo1Δ sgs1Δ* cells to an extent similar to that of *DDC1* deletion (Figure 1C). Thus, 9-1-1 failure to recruit Dpb11 to the damaged sites is sufficient to restore DNA damage resistance in *exo1Δ sgs1Δ* cells.

The Lack of Dpb11-Mediated Recruitment of Rad9 Suppresses the DNA Damage Sensitivity of *exo1Δ sgs1Δ* Cells

The 9-1-1 complex can recruit Dpb11 to sites of DNA lesions, which in turn interacts with Rad9 (referred to as the 9-1-1 axis) (Puddu et al., 2008; Pfander and Diffley, 2011) (Figure 1B). Dpb11-Rad9 interaction requires Cdk1-mediated phosphorylation of Rad9 Ser 462 and Thr 474 residues, which bind directly to the N-terminal BRCT repeats 1 and 2 of Dpb11 (Pfander and Diffley, 2011) (Figure 1B). To evaluate whether *exo1Δ sgs1Δ* suppression depends on the lack of Dpb11-Rad9 interaction, we used a *dpb11* allele lacking the BRCT1 and BRCT2 domains (*dpb11-ΔN*) and the *rad9-S462A*, *T474A* allele (*rad9-STAA*), encoding a Rad9 mutant variant that fails to interact with Dpb11 (Pfander and Diffley, 2011). Both *dpb11-ΔN* and *rad9-STAA* alleles were able to suppress the DNA damage hypersensitivity of *exo1Δ sgs1Δ* cells to extents similar to those of *dpb11-L410F* and *rad24Δ* alleles (Figure 1D), indicating that the lack of Dpb11-Rad9 interaction is responsible for the suppression.

Rad9 recruitment to sites of DNA damage relies also on Rad9 interaction with histone γH2A (Downs et al., 2000; Toh et al., 2006; Hammet et al., 2007) and with histone H3 methylated at Lys79 by the methyltransferase Dot1 (Wysocki et al., 2005; Grenon et al., 2007; Giannattasio et al., 2005). We investigated the contribution of these two pathways in the DNA damage sensitivity of *exo1Δ sgs1Δ* cells by analyzing the effect of abrogating Rad9 binding to H3-K79me or γH2A. The lack of *DOT1* (Figure S1A) or the expression of *hta1-S129A* (Figure S1B), which abolishes H3-K79me and γH2A generation, respectively, did

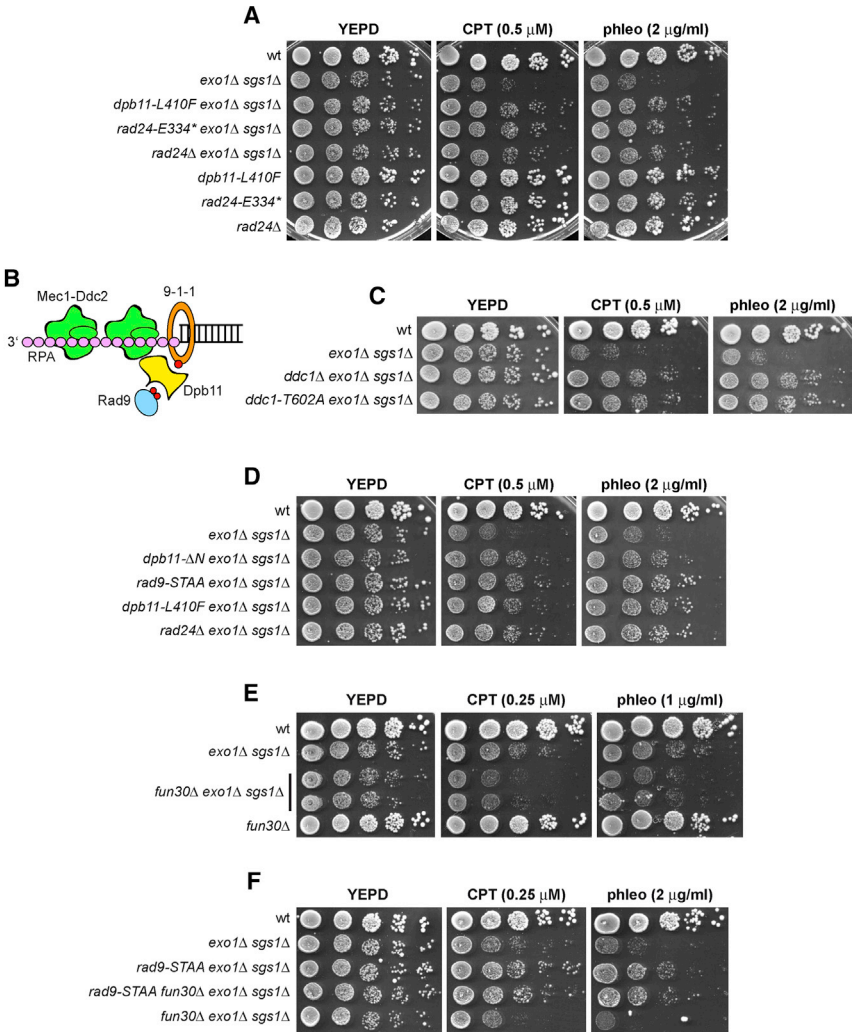

Figure 1. Failure of 9-1-1 to Recruit Dpb11 and Rad9 Partially Suppresses the DNA Damage Sensitivity of *exo1Δ sgs1Δ* Cells

(A) Exponentially growing cultures were serially diluted (1:10), and each dilution was spotted out onto YEPD (Yeast Extract-Peptone-Dextrose) plates with or without CPT or phleomycin.

(B) The 9-1-1 axis. The 9-1-1 complex recruits Dpb11 to the 5′ recessed end of a DSB, which in turn contributes to the association of Rad9 with DSBs. Red dots indicate phosphorylation events.

(C–F) Exponentially growing cultures were serially diluted (1:10), and each dilution was spotted out onto YEPD plates with or without CPT or phleomycin.

not suppress the DNA damage sensitivity of *exo1Δ sgs1Δ* cells. Rather, *hta1-S129A exo1Δ sgs1Δ* cells were more sensitive to DNA-damaging agents compared to *exo1Δ sgs1Δ* cells (Figure S1B). Altogether, these data indicate that Rad9 recruitment to damaged sites by Dpb11 is particularly detrimental in *exo1Δ sgs1Δ* cells.

The Lack of Fun30 Exacerbates the DNA Damage Sensitivity of *exo1Δ sgs1Δ* Cells in a Rad9-Dependent Manner

The Swr1-like family remodeler Fun30 (SMARCAD1 in mammals) interferes with Rad9 function at DSBs (Costelloe et al., 2012; Eapen et al., 2012; Bantele et al., 2017). In particular, the lack of Fun30 increases the association of Rad9 with DSBs (Chen et al., 2012; Dibitetto et al., 2016). The finding that Fun30 and Rad9 share the same interaction site on Dpb11 (Pfander and Diffley, 2011) suggests that Fun30 might interfere with Rad9 function by competition. We then investigated the effect of *FUN30* deletion in *exo1Δ sgs1Δ* cells. *FUN30* deletion exacerbated the DNA damage sensitivity of *exo1Δ sgs1Δ* cells (Figure 1E). The increased DNA damage sensitivity of *fun30Δ exo1Δ sgs1Δ* triple-mutant cells requires Rad9-Dpb11 interaction. In fact, *fun30Δ exo1Δ sgs1Δ* cells expressing the *rad9-STAA* allele, which abrogates Rad9-Dpb11 interaction and suppresses the DNA damage hypersensitivity of *exo1Δ sgs1Δ* cells, were as resistant to DNA-damaging agents as *rad9-STAA exo1Δ sgs1Δ* cells (Figure 1F). These findings further support the hypothesis that the Dpb11 function in recruiting Rad9 at sites of DNA lesions is detrimental when long-range resection is defective.

The Lack of Both Exo1 and Sgs1 Hyperactivates the Checkpoint in Response to DNA Damaging Agents

DSB formation leads to the activation of a checkpoint response that depends primarily on Mec1, which binds RPA-coated ssDNA and promotes Rad53 activation (Zou and Elledge, 2003). Rad9 links the signal transduction from Mec1 to Rad53 by acting as a scaffold to allow Rad53 intermolecular autophosphorylation and activation (Gilbert et al., 2001; Sweeney et al., 2005; Schwartz et al., 2002).

The lack of both Exo1 and Sgs1 has been reported to impair Rad53 activation in response to a single site-specific DSB (Zhu et al., 2008; Gravel et al., 2008; Bantele et al., 2019). Thus, we evaluated the ability of *exo1Δ sgs1Δ* cells to phosphorylate Rad53 not only after generation of a single DSB but also after genotoxic treatments. To induce a single unrepaired DSB, we used JKM139 derivative strains that express the site-specific HO (homothallic switching) endonuclease gene from a galactose-inducible promoter (Lee et al., 1998). Galactose addition leads to HO induction that catalyzes a single DSB at the *MAT* locus. The HO cut cannot be repaired by HR, because the homologous donor sequences *HML* and *HMR* are deleted. Consistent with previous data (Zhu et al., 2008; Gravel et al., 2008; Bantele et al., 2019), Rad53 phosphorylation, which is required for checkpoint activation and is detectable as a

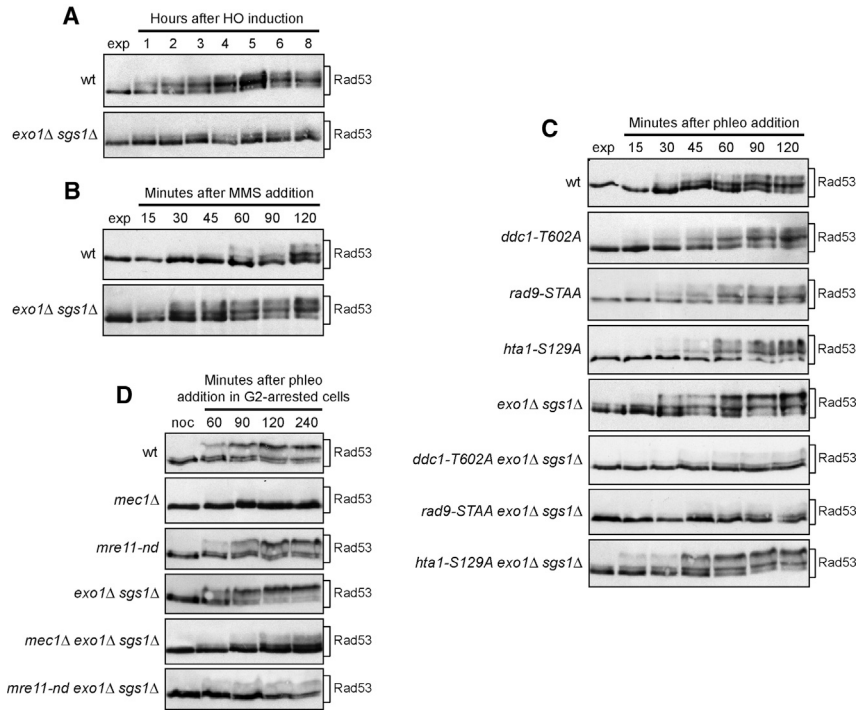

Figure 2. Checkpoint Activation in *exo1Δ sgs1Δ* Cells Depends Primarily on 9-1-1 Function in Recruiting Dpb11 and Rad9 at Damaged DNA

(A) *HO* expression was induced after galactose addition and protein extracts were analyzed by western blot using anti-Rad53 antibodies.

(B and C) MMS (0.015%) (B) or phleomycin (10 μg/mL) (C) was added to exponentially growing cells, and protein extracts were analyzed by western blot using anti-Rad53 antibodies.

(D) Phleomycin (10 μg/mL) and nocodazole (15 μg/mL) were added to nocodazole-arrested cell cultures. Protein extracts were analyzed by western blot using anti-Rad53 antibodies.

decrease of Rad53 electrophoretic mobility, was lower in *exo1Δ sgs1Δ* cells than in wild-type cells after HO induction (Figure 2A). By contrast, when methylmethane sulphonate (MMS) or phleomycin was added to exponentially growing cells, Rad53 phosphorylation was higher in *exo1Δ sgs1Δ* cells than in wild-type cells (Figures 2B and 2C). A certain level of Rad53 phosphorylation was detectable in *exo1Δ sgs1Δ* cells even in the absence of DNA damage, possibly due to DNA replication defects (Figures 2B and 2C).

Interestingly, replication of damaged DNA template is not responsible for checkpoint activation in phleomycin-treated *exo1Δ sgs1Δ* cells. In fact, significant changes in Rad53 electrophoretic mobility could be detected after phleomycin treatment of G2-arrested *exo1Δ sgs1Δ* cells that were kept arrested in G2 after phleomycin addition (Figure 2D). This Rad53 phosphorylation depends mainly on Mec1, as Rad53 phosphorylation was dramatically reduced when phleomycin was added to G2-arrested *mec1Δ exo1Δ sgs1Δ* cells (kept viable by *SML1* deletion) (Figure 2D). Since Mec1 is known to activate Rad53 in a manner that strongly depends on ssDNA length (Pellicioli et al., 2001; Bantele et al., 2019), this finding suggests that nucleases other than Exo1 and Dna2 are responsible for ssDNA generation to induce Mec1 activation in *exo1Δ sgs1Δ* cells. DSB resection in *exo1Δ sgs1Δ* cells depends on Mre11 nuclease activity (Zhu et al., 2008; Mimitou and Symington, 2008), and phleomycin addition failed to induce Rad53 phosphorylation in G2-arrested *exo1Δ sgs1Δ* cells expressing the *mre11-H125N* nuclease-dead allele (*mre11-nd*) (Figure 2D). This finding indicates that the Mre11 processing activity is responsible for ssDNA generation and checkpoint activation in *exo1Δ sgs1Δ* cells. Since resection in *exo1Δ sgs1Δ* cells by Mre11 nuclease is limited to the vicinity of the DSB ends (Zhu et al., 2008; Mimitou and Symington, 2008), the amount of ssDNA generated at the ends of a single DSB could not reach the threshold level for Mec1 activation, thus explaining the inability of *exo1Δ sgs1Δ* cells to activate the checkpoint in response to a single DSB. By contrast, processing by Mre11 nuclease of the multiple DNA lesions caused by exposure to DNA-damaging agents should generate higher total amount of ssDNA that can be enough to activate Mec1.

The Lack of 9-1-1 Axis Suppresses the DNA Damage Sensitivity of *exo1Δ sgs1Δ* Cells by Dampening Rad53 Activation

Rad9 is recruited to chromatin by binding to H3-K79me, γH2A, and Dpb11 (Puddu et al., 2008; Mordes et al., 2008; Navadgi-Patil and Burgers, 2008; Pfander and Diffley, 2011). Previous studies have shown that Dpb11 acts redundantly with Dot1 in promoting Rad53 activation in response to genotoxic treatments (Puddu et al., 2008; Pfander and Diffley, 2011). Consistent with this finding, Rad53 phosphorylation in phleomycin-treated *ddc1-T602A* and *rad9-STAA* cells was similar to that observed in wild-type cells (Figure 2C). Surprisingly, the presence of either the *rad9-STAA* or the *ddc1-T602A* allele dramatically decreased Rad53 phosphorylation in phleomycin-treated *exo1Δ sgs1Δ* cells compared to not only *exo1Δ sgs1Δ* cells but also wild-type cells (Figure 2C). By contrast, the *hta1-S129A* allele did not decrease Rad53 phosphorylation in response to phleomycin addition in either the presence or absence of Exo1 and Sgs1 (Figure 2C). Altogether, these findings indicate that *exo1Δ sgs1Δ* cells activate a checkpoint in response to genotoxic treatments that is stronger than wild-type cells and that depends primarily on the 9-1-1 axis.

The importance of the 9-1-1 axis in Rad53 activation in *exo1Δ sgs1Δ* cells prompted us to investigate whether the *ddc1-T602A* and *rad9-STAA* alleles restore DNA damage resistance of *exo1Δ sgs1Δ* cells by dampening the checkpoint response. If this were the case, then inactivation of Rad53 kinase activity should restore DNA damage resistance of *exo1Δ sgs1Δ* cells.

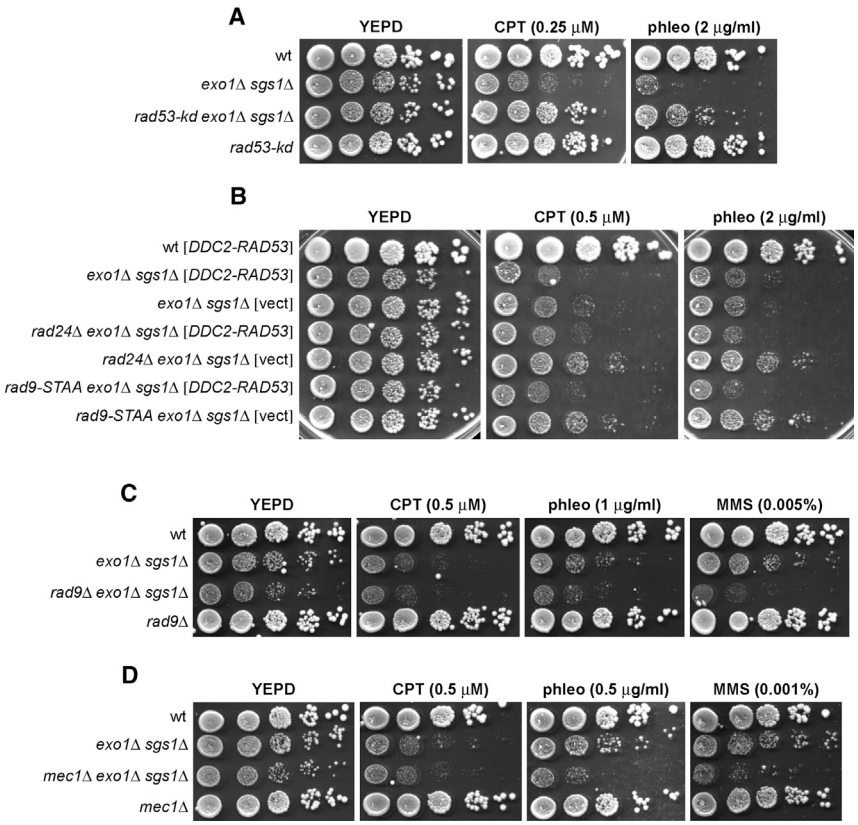

Figure 3. Dampening Rad53 Activation Suppresses the DNA Damage Sensitivity of *exo1Δ sgs1Δ* Cells

(A–D) Exponentially growing cultures were serially diluted (1:10), and each dilution was spotted out onto YEPD plates with or without CPT, phleomycin, or MMS.

Furthermore, enforcing Rad53 recruitment to damaged DNA independently of both Rad9 and 9-1-1 by fusing Rad53 with the Mec1 regulatory subunit Ddc2 (Lee et al., 2004) should resensitize *rad24Δ exo1Δ sgs1Δ* and *rad9-STAA exo1Δ sgs1Δ* mutants to DNA-damaging agents. Indeed, we found that expression of the *rad53-K227A* (*rad53-kd*) allele, which specifically impairs Rad53 kinase activity, suppressed the sensitivity of *exo1Δ sgs1Δ* cells to CPT and phleomycin treatments (Figure 3A). Furthermore, *rad24Δ exo1Δ sgs1Δ* and *rad9-STAA exo1Δ sgs1Δ* mutants, transformed with a plasmid carrying a *DDC2-RAD53* in-frame fusion, were more sensitive to DNA-damaging agents than *rad9-STAA exo1Δ sgs1Δ* and *rad24Δ exo1Δ sgs1Δ* mutants transformed with an empty vector (Figure 3B). These findings indicate that checkpoint hyperactivation can account for the increased DNA damage sensitivity of *exo1Δ sgs1Δ* cells and that the lack of 9-1-1 ability to recruit Dpb11 and Rad9 at damaged sites can restore DNA damage resistance of *exo1Δ sgs1Δ* cells by inhibiting checkpoint activation.

Interestingly, neither *RAD9* nor *MEC1* deletion suppressed the DNA damage hypersensitivity of *exo1Δ sgs1Δ* cells (Figures 3C and 2D). Rather, both *rad9Δ exo1Δ sgs1Δ* and *mec1Δ exo1Δ sgs1Δ* triple mutants (kept viable by *SML1* deletion) were more sensitive to phleomycin and MMS than *exo1Δ sgs1Δ* cells (Figures 3C and 3D), suggesting that Rad9 and Mec1 have additional Rad53-independent functions in supporting DNA damage resistance of *exo1Δ sgs1Δ* cells.

The 9-1-1 Complex Inhibits Short-Range Resection by Restricting Mre11 Nuclease

Resection in *exo1Δ sgs1Δ* cells is limited to the vicinity of the DSB end and depends on Mre11 nuclease activity (Zhu et al., 2008; Mimitou and Symington, 2008). To exclude possible effects of 9-1-1, Rad9, or Rad53 on DSB resection in *exo1Δ sgs1Δ* cells, we used JKM139 derivative strains, where a single irreparable DSB at the *MAT* locus can be generated by expressing the HO endonuclease gene (Lee et al., 1998). Resection of DNA regions flanking the HO-induced DNA break renders the DNA sequence resistant to cleavage by restriction enzymes, resulting in the appearance of resection intermediates (r1–r6) that can be detected by Southern blot analysis with a probe that anneals to the 3′ end at one side of the break (Figure S2A). Consistent with previous data showing that only 30% of *exo1Δ sgs1Δ* cells process DSB ends beyond 100 or 200 nt 4 h after HO induction (Zhu et al., 2008), only the r1 resection product was barely detectable in *exo1Δ sgs1Δ* cells and did not accumulate throughout the experiment (Figure 4A–4C), indicating that resection in most cells failed to proceed beyond the SspI site located 0.9 kb from the HO cut site. By contrast, the r1 resection product accumulated much more abundantly in both *ddc1Δ exo1Δ sgs1Δ* (Figures 4A and 4C) and *rad24Δ exo1Δ sgs1Δ* cells (Figures 4B and 4C) compared to *exo1Δ sgs1Δ* cells, indicating that most cells were capable of resecting the HO-induced DSB beyond 0.9 kb from the HO cutting site. Furthermore, both *ddc1Δ exo1Δ sgs1Δ* and *rad24Δ exo1Δ sgs1Δ* cells showed appearance of the r2 resection product (Figures 4A–4C), indicating that resection in some cells proceeded beyond the SspI site located 1.7 kb from the HO cleavage site.

Consistent with a more extensive resection in *ddc1Δ exo1Δ sgs1Δ* and *rad24Δ exo1Δ sgs1Δ* cells compared to *exo1Δ sgs1Δ*, Rad50 chromatin immunoprecipitation (ChIP) signals were greatly enriched in sequences within a few hundred nucleotides of the DSB in *exo1Δ sgs1Δ* and decreased rapidly with increasing distance from the break site (Figure 4D). By contrast, although it has to be considered that resolution of the ChIP signals depends on the DNA fragment sizes (200–1,000 bp) obtained after sonication, Rad50 signals close to the break site were lower in both *ddc1Δ exo1Δ sgs1Δ* and *rad24Δ exo1Δ sgs1Δ* than in *exo1Δ sgs1Δ* cells. Furthermore, they were

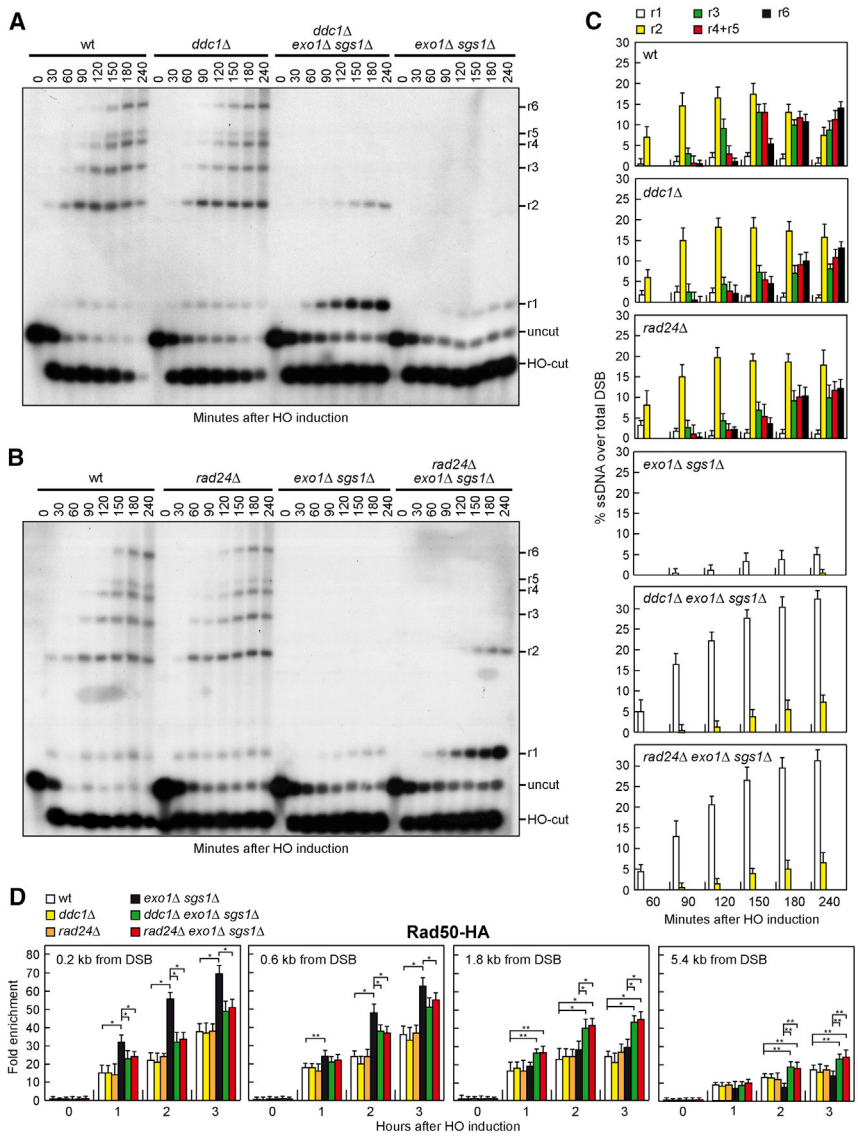

Figure 4. The Lack of Ddc1 or Rad24 Extends DSB Resection in *exo1Δ sgs1Δ* Cells

(A and B) YEPR (Yeast Extract-Peptone-Raffinose) exponentially growing cell cultures were transferred to YEPRG (Yeast Extract-Peptone-Raffinose-Galactose) at time 0 to induce *HO* expression. SspI-digested genomic DNA separated on alkaline agarose gel was hybridized with a single-stranded *MAT* probe that anneals with the unresected strand. 5′–3′ resection progressively eliminates SspI sites, producing longer SspI fragments (r1–r6) detected by the probe.

(C) Densitometric analysis. The experiment (as in A and B) was independently repeated three times, and mean values are represented, with error bars denoting SD.

(D) ChIP and qPCR. Exponentially growing YEPR cell cultures were transferred to YEPRG to induce HO expression, followed by ChIP analysis of the recruitment of Rad50-HA at the indicated distance from the HO cut. In all diagrams, ChIP signals were normalized for each time point to the corresponding input signal. The mean values of three independent experiments are represented, with error bars denoting SD. *$p < 0.005$; **$p < 0.05$ (Student's t test).

present at higher levels in DNA sequences 1.8 and 5.4 kb from the DSB (Figure 4D).

Interestingly, inhibition of DSB resection by the 9-1-1 complex appears to occur independently of Rad53 activation and 9-1-1 function in recruiting Dpb11 and Rad9. In fact, although our assay did not allow us to detect differences in ssDNA generation within 0.9 kb of the HO cutting site, the *rad9-STAA*, *ddc1-T602*, and *rad53-kd* alleles did not appear to extend resection in *exo1Δ sgs1Δ* cells (Figure S2B).

Resection in *exo1Δ sgs1Δ* cells depends on Mre11 nuclease activity (Zhu et al., 2008; Mimitou and Symington, 2008). Expression of the *mre11-H125N* nuclease-dead allele (*mre11-nd*) reduced resection of the HO-induced DSB to undetectable level not only in *exo1Δ sgs1Δ* cells but also in *ddc1Δ exo1Δ sgs1Δ* cells (Figures 5A and 5B), indicating that the enhanced resection in *ddc1Δ exo1Δ sgs1Δ* cells is due to Mre11 nuclease activity.

The 3′ ssDNA tails generated by resection are converted to Rad51-coated nucleoprotein filaments that invade a duplex repair template to generate a region of heteroduplex DNA (hetDNA), where the invading strand is paired with the complementary strand (Guo et al., 2017). Interestingly, the lack of both Exo1 and Sgs1 was shown to cause a ~10-fold reduction of ectopic recombination by decreasing hetDNA length (Guo et al., 2017). To test the effect of *DDC1* and *RAD24* deletion on ectopic recombination, we used a *LYS2*-based assay, where the recipient allele was constructed by inserting an I-*Sce*I cleavage site into the endogenous *LYS2* locus, the insertion of which creates a frameshift mutation (Guo et al., 2017). As repair donor, a 3′-truncated *lys2* allele (*lys2Δ3′*), which contains a non-cleavable I-*Sce*I site due to a 4-bp duplication, was integrated at the *CAN1* locus. During repair, the 4-bp duplication in the donor allele is copied into the recipient allele, producing Lys^+ recombinant clones. Consistent with previous findings (Mimitou and Symington, 2008; Chung et al., 2010; Guo et al., 2017), *exo1Δ sgs1Δ* cells showed an ~10 fold decrease in the frequency of Lys^+ clones compared to wild-type (Figure 5C). In agreement with a role of 9-1-1 in inhibiting DSB resection in *exo1Δ sgs1Δ* cells independently of Rad9 and Rad53, Lys^+ recombination frequency increased in both *rad24Δ exo1Δ sgs1Δ* and *ddc1Δ exo1Δ sgs1Δ* triple mutants compared to *exo1Δ sgs1Δ* cells (Figure 5C). By contrast, the *rad9-STAA* and *rad53-kd* alleles, which did not appear to extend resection in *exo1Δ sgs1Δ* cells, did not increase *exo1Δ sgs1Δ* Lys^+ recombination frequency (Figure 5C).

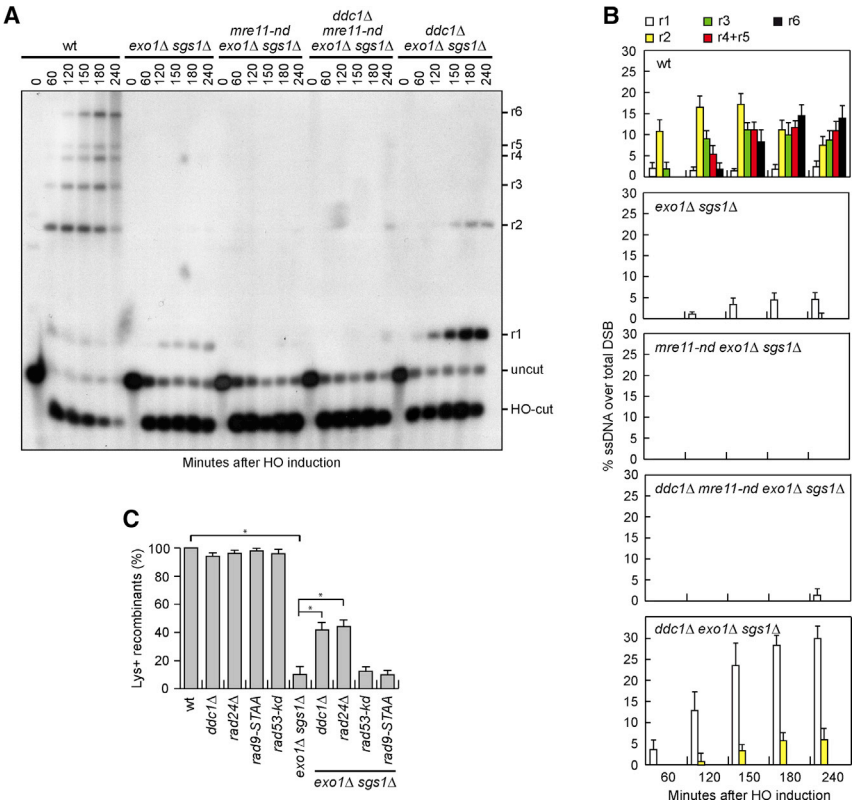

Figure 5. DSB Resection in *ddc1Δ exo1Δ sgs1Δ* Cells Depends on Mre11 Nuclease

(A) YEPR exponentially growing cell cultures were transferred to YEPRG at time 0 to induce *HO* expression. SspI-digested genomic DNA separated on alkaline agarose gel was hybridized as described in Figure 4A.

(B) Densitometric analysis. The experiment (as in A) was independently repeated three times, and mean values are represented, with error bars denoting SD.

(C) Recombination frequency. I-SceI expression was induced by galactose addition. Cells were plated on YEPD and SC-lys (Synthetic Complete without lysine) media, and repair frequencies were calculated as the ratio of Lys^+ to total colonies in at least three independent experiments, with 15 independent cultures per experiment. Data are expressed as percentage of Lys^+ colonies relative to wild-type that was set up at 100%, with error bars denoting SD. *$p < 0.005$ (Student's t test).

DISCUSSION

A previous study showed that the 9-1-1 complex inhibits the activity of long-range resection nucleases by promoting the association of Rad9 with DSBs (Ngo and Lydall, 2015). Here, we provide evidence that Rad9 recruitment to damaged DNA by the 9-1-1 complex plays a key role in activating the checkpoint in response to DNA-damaging agents when long-range resection is abrogated by the lack of both Exo1 and Sgs1. This checkpoint activation, which requires both Mre11 nuclease activity and Mec1, contributes to increase the DNA damage sensitivity of *exo1Δ sgs1Δ* cells. In fact, failure of 9-1-1 to recruit Dpb11 and Rad9 at DSBs, but not abrogation of the association of Rad9 with γH2A and H3K79me, partially restores DNA damage resistance of *exo1Δ sgs1Δ* cells.

It is worth pointing out that while γH2A and H3K79me spread kilobases around the lesion and throughout euchromatin, respectively (Shroff et al., 2004; Nguyen and Zhang, 2011), the 9-1-1 complex is loaded at the ssDNA-dsDNA junction (Majka and Burgers, 2003; Majka et al., 2006). Furthermore, the 3′ ssDNA tail stemming from the short-range resection is expected to be bound by RPA, which was shown to promote 9-1-1 foci formation (Lisby et al., 2004). The finding that the 9-1-1 axis appears to be more specifically located at damaged DNA could explain the specific involvement of 9-1-1 in activating the checkpoint in *exo1Δ sgs1Δ* cells. Thus, we propose that MRX and Sae2 start resection in *exo1Δ sgs1Δ* cells, generating a recessed 5′ end structure for 9-1-1, Dpb11, and Rad9 loading. This initial resection is suboptimal for DSB repair by HR, causing persistent Rad53-mediated cell-cycle arrest that depends primarily on 9-1-1 and decreases survival to genotoxic treatments (Figure 6).

Interestingly, the lack of either Rad9 or Mec1 not only fails to restore DNA damage resistance of *exo1Δ sgs1Δ* cells but also exacerbates their DNA damage sensitivity, suggesting that Rad9 and Mec1 play a role in DSB repair independently of their function in checkpoint activation. Consistent with this hypothesis, Rad9 was shown to promote long-tract gene conversion, crossover recombination, and break-induced replication by facilitating stable annealing between the recombinogenic filament and the donor template (Ferrari et al., 2020).

In addition of inhibiting Exo1 and Dna2-Sgs1 activity by promoting Rad9 association at DSBs (Ngo and Lydall, 2015), the 9-1-1 complex also negatively regulates MRX-mediated short-range resection. In fact, the lack of either Rad24 or the Ddc1 subunit of 9-1-1 partially suppresses the resection defect and increases recombination frequency of *exo1Δ sgs1Δ* cells. DSB resection in *ddc1Δ exo1Δ sgs1Δ* requires Mre11 nuclease activity, indicating that the 9-1-1 clamp restricts MRX-mediated resection of DSB ends.

Although our assay does not allow to detect differences in ssDNA generation very close to the break site, this control of MRX processing activity does not seem to rely on 9-1-1 recruitment of Dpb11 and Rad9, as the *ddc1-T602A* and *rad9-STAA* alleles are not capable of extending resection in *exo1Δ sgs1Δ* cells. Furthermore, *rad9-STAA* does not increase the recombination frequency of *exo1Δ sgs1Δ* cells. The extent of suppression of the DNA damage sensitivity of *exo1Δ sgs1Δ* by the *rad9-STAA* allele, which downregulates checkpoint activation but does not appear to extend DSB resection in *exo1Δ sgs1Δ* cells, is similar to that caused by the lack of Rad24 or Ddc1. This finding suggests that loss of the checkpoint rather than a more extensive resection plays the major role in increasing

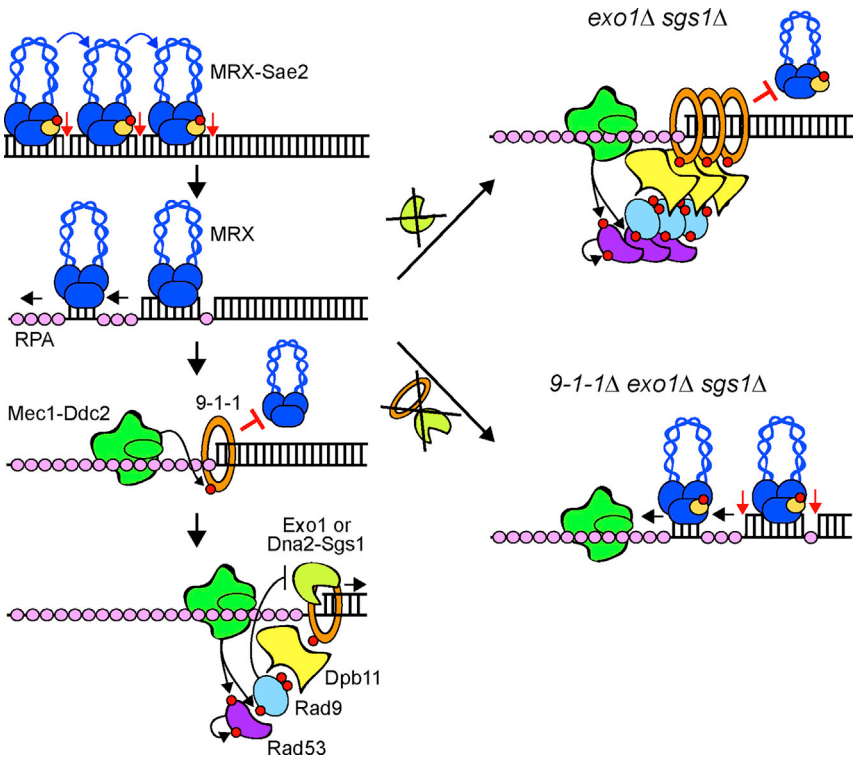

Figure 6. Model for 9-1-1 Function during Short-Range Resection

MRX, aided by phosphorylated Sae2, promotes cleavage (red arrows) of dsDNA by another MRX complex that binds DNA at an adjacent site (blue arrows). The nicks are followed by exonucleolytic degradation of the DNA between the incision sites (black arrows). When a certain amount of ssDNA coated by RPA is generated, the loading of 9-1-1 at the ssDNA-dsDNA junction is allowed and limits MRX diffusion and additional MRX-mediated DNA cleavage events. Exo1 and Dna2-Sgs1 extend the resected tracts. The generation of RPA-coated ssDNA allows the recruitment of Mec1-Ddc2, which creates a docking site on 9-1-1 for Dpb11 binding. Dpb11 in turn engages interactions with Rad9 and Mec1-Ddc2 to allow Rad53 phosphorylation and activation. Rad9 and Rad53, in turn, inhibit the activity of Exo1 and Dna2-Sgs1. In the absence of both Exo1 and Dna2-Sgs1 (*exo1⊿ sgs1⊿*), accumulation of short 3′ ssDNA tails generated by Mre11 nuclease leads to an increased association of 9-1-1 with the ss-dsDNA junction, which leads to Dpb11- and Rad9-mediated Rad53 hyperactivation that decreases DNA damage resistance. The absence of 9-1-1 in *exo1⊿ sgs1⊿* cells (*exo1⊿ sgs1⊿ 9-1-1⊿*) prevents checkpoint activation and allows the sliding on dsDNA of MRX, which catalyzes additional cleavage events. Red dots indicate phosphorylation events.

DNA damage resistance of *ddc1⊿ exo1*Δ *sgs1*Δ and *rad24⊿ exo1*Δ *sgs1*Δ cells. Although the short ssDNA tails resulting from MRX-Sae2-dependent cleavage result only in a moderate decrease of ectopic recombination (Mimitou and Symington, 2008; Westmoreland and Resnick, 2016; Zhu et al., 2008), the lack of both Exo1 and Sgs1 might cause the persistence of DNA lesions that are not lethal by themselves but whose processing can activate a checkpoint that decreases DNA damage resistance by causing a persistent cell-cycle arrest.

The control of MRX nuclease activity in the vicinity of DSB ends is poorly understood. In *exo1⊿ sgs1⊿* cells, the MRX-dependent resection can reach up to 100–300 nt possibly resulting from multiple MRX-Sae2-dependent cleavage events (Mimitou and Symington, 2008; Zhu et al., 2008; Guo et al., 2017). Consistent with this hypothesis, a recent reconstitution of the *S. cerevisiae* short-range resection machinery revealed the ability of MRX-Sae2 to resect the 5′-terminated strand at DSBs in a stepwise manner, in which one MRX-Sae2 ensemble stimulates DNA cleavage by another MRX-Sae2 ensemble that is bound at adjacent sites internal to the DSB (Cannavo et al., 2019). The 3′–5′ exonucleolytic activity is then limited to degrading DNA between the endonucleolytic incision sites.

Interestingly, the 9-1-1 complex is known to associate at the ssDNA-dsDNA junctions in a resection-dependent manner (Ellison and Stillman, 2003; Majka and Burgers, 2003; Majka et al., 2006; Bantele et al., 2019). Furthermore, both 9-1-1 and MRX are capable of sliding along dsDNA (Majka and Burgers, 2003; Myler et al., 2017). Our finding that the 9-1-1 complex negatively regulates Mre11 nuclease suggests a model whereby the generation of ssDNA by MRX-mediated stepwise incision allows the loading to the resection border of the 9-1-1 complex, which, by sliding on dsDNA, might limit MRX diffusion and therefore additional cleavage events (Figure 6). Consistent with such a function, Rad50 ChIP signals, which accumulated in *exo1*Δ *sgs1*Δ very close to the break site, were broader distributed and persisted longer with increasing distance from the DSB end in both *ddc1⊿ exo1*Δ *sgs1*Δ and *rad24⊿ exo1*Δ *sgs1*Δ cells than in *exo1*Δ *sgs1*Δ cells. 9-1-1 binding to the DSB ends also recruits Dpb11, which in turn provides a scaffolding function for Rad9 and Mec1-Ddc2, to form a protein complex that allows Rad53 activation in proximity to DNA lesions (Figure 6) (Gilbert et al., 2001; Sweeney et al., 2005; Schwartz et al., 2002).

In conclusion, our findings reveal that the 9-1-1 complex, in addition to regulating long-range resection nucleases (Ngo and Lydall, 2015), also inhibits short-range resection by restricting MRX nuclease activity to prevent unscheduled DNA degradation. Furthermore, the 9-1-1 function in recruiting Dpb11 and Rad9 can couple the control of DSB resection with checkpoint activation. Since the 9-1-1 complex is evolutionarily conserved, it will be interesting to investigate whether a similar regulatory mechanism on DSB resection and checkpoint activation also occurs in mammalian cells.

STAR★METHODS

Detailed methods are provided in the online version of this paper and include the following:

- KEY RESOURCES TABLE

SUPPLEMENTAL INFORMATION

Supplemental Information can be found online at https://doi.org/10.1016/j.celrep.2020.108287.

ACKNOWLEDGMENTS

We thank J. Diffley, J. Haber, S. Jinks-Robertson, G. Ira, and B. Pfander for yeast strains; D. Stern for plasmids; and G. Lucchini for critical reading of the manuscript. This work was supported by Fondazione AIRC under IG 2017 - ID 19783 project (M.P.L., principal investigator) and Progetti di Ricerca di Interesse Nazionale (PRIN) 2017 (M.P.L. and D.B.). E.C. was supported by a fellowship from the Ministry of Education, University and Research (MIUR) through the grant Dipartimenti di Eccellenza-2017.

AUTHOR CONTRIBUTIONS

E.G. and M.P.L. designed the experiments. E.G., E.C., and C.V.C performed the experiments. E.G., D.B., and M.P.L. analyzed the data. M.P.L. wrote the paper. E.G., E.C., and D.B. revised the manuscript.

DECLARATION OF INTERESTS

The authors declare no competing interests.

Received: June 21, 2020
Revised: September 8, 2020
Accepted: September 28, 2020
Published: October 20, 2020

REFERENCES

Bantele, S.C.S., Ferriera, P., Gritenaite, D., Boos, D., and Pfander, B. (2017). Targeting of the Fun30 nucleosome remodeller by the Dpb11 scaffold facilitates cell cycle-regulated DNA end resection. eLife *6*, e21687.

Bantele, S.C.S., Lisby, M., and Pfander, B. (2019). Quantitative sensing and signalling of single-stranded DNA during the DNA damage response. Nat. Commun. *10*, 944.

Bonetti, D., Villa, M., Gobbini, E., Cassani, C., Tedeschi, G., and Longhese, M.P. (2015). Escape of Sgs1 from Rad9 inhibition reduces the requirement for Sae2 and functional MRX in DNA end resection. EMBO Rep. *16*, 351–361.

Bonetti, D., Colombo, C.V., Clerici, M., and Longhese, M.P. (2018). Processing of DNA ends in the maintenance of genome stability. Front. Genet. *9*, 390.

Cannavo, E., and Cejka, P. (2014). Sae2 promotes dsDNA endonuclease activity within Mre11-Rad50-Xrs2 to resect DNA breaks. Nature *514*, 122–125.

Cannavo, E., Cejka, P., and Kowalczykowski, S.C. (2013). Relationship of DNA degradation by *Saccharomyces cerevisiae* Exonuclease 1 and its stimulation by RPA and Mre11-Rad50-Xrs2 to DNA end resection. Proc. Natl. Acad. Sci. USA *110*, E1661–E1668.

Cannavo, E., Reginato, G., and Cejka, P. (2019). Stepwise 5′ DNA end-specific resection of DNA breaks by the Mre11-Rad50-Xrs2 and Sae2 nuclease ensemble. Proc. Natl. Acad. Sci. USA *116*, 5505–5513.

Cassani, C., Gobbini, E., Wang, W., Niu, H., Clerici, M., Sung, P., and Longhese, M.P. (2016). Tel1 and Rif2 regulate MRX function in end-tethering and repair of DNA double-strand breaks. PLoS Biol. *14*, e1002387.

Cejka, P., Cannavo, E., Polaczek, P., Masuda-Sasa, T., Pokharel, S., Campbell, J.L., and Kowalczykowski, S.C. (2010). DNA end resection by Dna2-Sgs1-RPA and its stimulation by Top3-Rmi1 and Mre11-Rad50-Xrs2. Nature *467*, 112–116.

Chen, X., Cui, D., Papusha, A., Zhang, X., Chu, C.D., Tang, J., Chen, K., Pan, X., and Ira, G. (2012). The Fun30 nucleosome remodeller promotes resection of DNA double-strand break ends. Nature *489*, 576–580.

Chung, W.H., Zhu, Z., Papusha, A., Malkova, A., and Ira, G. (2010). Defective resection at DNA double-strand breaks leads to de novo telomere formation and enhances gene targeting. PLoS Genet. *6*, e1000948.

Clerici, M., Trovesi, C., Galbiati, A., Lucchini, G., and Longhese, M.P. (2014). Mec1/ATR regulates the generation of single-stranded DNA that attenuates Tel1/ATM signaling at DNA ends. EMBO J. *33*, 198–216.

Costelloe, T., Louge, R., Tomimatsu, N., Mukherjee, B., Martini, E., Khadaroo, B., Dubois, K., Wiegant, W.W., Thierry, A., Burma, S., et al. (2012). The yeast Fun30 and human SMARCAD1 chromatin remodellers promote DNA end resection. Nature *489*, 581–584.

Cussiol, J.R., Jablonowski, C.M., Yimit, A., Brown, G.W., and Smolka, M.B. (2015). Dampening DNA damage checkpoint signalling via coordinated BRCT domain interactions. EMBO J. *34*, 1704–1717.

Delacroix, S., Wagner, J.M., Kobayashi, M., Yamamoto, K., and Karnitz, L.M. (2007). The Rad9-Hus1-Rad1 (9-1-1) clamp activates checkpoint signaling via TopBP1. Genes Dev. *21*, 1472–1477.

Dibitetto, D., Ferrari, M., Rawal, C.C., Balint, A., Kim, T., Zhang, Z., Smolka, M.B., Brown, G.W., Marini, F., and Pellicioli, A. (2016). Slx4 and Rtt107 control checkpoint signalling and DNA resection at double-strand breaks. Nucleic Acids Res. *44*, 669–682.

Downs, J.A., Lowndes, N.F., and Jackson, S.P. (2000). A role for *Saccharomyces cerevisiae* histone H2A in DNA repair. Nature *408*, 1001–1004.

Eapen, V.V., Sugawara, N., Tsabar, M., Wu, W.H., and Haber, J.E. (2012). The *Saccharomyces cerevisiae* chromatin remodeler Fun30 regulates DNA end resection and checkpoint deactivation. Mol. Cell. Biol. *32*, 4727–4740.

Ellison, V., and Stillman, B. (2003). Biochemical characterization of DNA damage checkpoint complexes: clamp loader and clamp complexes with specificity for 5′ recessed DNA. PLoS Biol. *1*, E33.

Ferrari, M., Dibitetto, D., De Gregorio, G., Eapen, V.V., Rawal, C.C., Lazzaro, F., Tsabar, M., Marini, F., Haber, J.E., and Pellicioli, A. (2015). Functional interplay between the 53BP1-ortholog Rad9 and the Mre11 complex regulates resection, end-tethering and repair of a double-strand break. PLoS Genet. *11*, e1004928.

Ferrari, M., Rawal, C.C., Lodovichi, S., Vietri, M.Y., and Pellicioli, A. (2020). Rad9/53BP1 promotes DNA repair via crossover recombination by limiting the Sgs1 and Mph1 helicases. Nat. Commun. *11*, 3181.

Garcia, V., Phelps, S.E.L., Gray, S., and Neale, M.J. (2011). Bidirectional resection of DNA double-strand breaks by Mre11 and Exo1. Nature *479*, 241–244.

Giannattasio, M., Lazzaro, F., Plevani, P., and Muzi-Falconi, M. (2005). The DNA damage checkpoint response requires histone H2B ubiquitination by Rad6-Bre1 and H3 methylation by Dot1. J. Biol. Chem. *280*, 9879–9886.

Gilbert, C.S., Green, C.M., and Lowndes, N.F. (2001). Budding yeast Rad9 is an ATP-dependent Rad53 activating machine. Mol. Cell *8*, 129–136.

Granata, M., Lazzaro, F., Novarina, D., Panigada, D., Puddu, F., Abreu, C.M., Kumar, R., Grenon, M., Lowndes, N.F., Plevani, P., et al. (2010). Dynamics of Rad9 chromatin binding and checkpoint function are mediated by its dimerization and are cell cycle-regulated by CDK1 activity. PLoS Genet. *6*, e1001047.

Gravel, S., Chapman, J.R., Magill, C., and Jackson, S.P. (2008). DNA helicases Sgs1 and BLM promote DNA double-strand break resection. Genes Dev. *22*, 2767–2772.

Grenon, M., Costelloe, T., Jimeno, S., O'Shaughnessy, A., Fitzgerald, J., Zgheib, O., Degerth, L., and Lowndes, N.F. (2007). Docking onto chromatin via the *Saccharomyces cerevisiae* Rad9 Tudor domain. Yeast *24*, 105–119.

Guo, X., Hum, Y.F., Lehner, K., and Jinks-Robertson, S. (2017). Regulation of hetDNA length during mitotic double-strand break repair in yeast. Mol. Cell *67*, 539–549.e4.

Hammet, A., Magill, C., Heierhorst, J., and Jackson, S.P. (2007). Rad9 BRCT domain interaction with phosphorylated H2AX regulates the G1 checkpoint in budding yeast. EMBO Rep. *8*, 851–857.

Keelagher, R.E., Cotton, V.E., Goldman, A.S., and Borts, R.H. (2011). Separable roles for Exonuclease I in meiotic DNA double-strand break repair. DNA Repair (Amst.) *10*, 126–137.

Kowalczykowski, S.C. (2015). An overview of the molecular mechanisms of recombinational DNA repair. Cold Spring Harb. Perspect. Biol. *7*, a016410.

Lazzaro, F., Sapountzi, V., Granata, M., Pellicioli, A., Vaze, M., Haber, J.E., Plevani, P., Lydall, D., and Muzi-Falconi, M. (2008). Histone methyltransferase Dot1 and Rad9 inhibit single-stranded DNA accumulation at DSBs and uncapped telomeres. EMBO J. *27*, 1502–1512.

Lee, S.E., Moore, J.K., Holmes, A., Umezu, K., Kolodner, R.D., and Haber, J.E. (1998). *Saccharomyces* Ku70, Mre11/Rad50 and RPA proteins regulate adaptation to G2/M arrest after DNA damage. Cell *94*, 399–409.

Lee, S.J., Duong, J.K., and Stern, D.F. (2004). A Ddc2-Rad53 fusion protein can bypass the requirements for *RAD9* and *MRC1* in Rad53 activation. Mol. Biol. Cell *15*, 5443–5455.

Lisby, M., Barlow, J.H., Burgess, R.C., and Rothstein, R. (2004). Choreography of the DNA damage response: spatiotemporal relationships among checkpoint and repair proteins. Cell *118*, 699–713.

Majka, J., and Burgers, P.M.J. (2003). Yeast Rad17/Mec3/Ddc1: a sliding clamp for the DNA damage checkpoint. Proc. Natl. Acad. Sci. USA *100*, 2249–2254.

Majka, J., Binz, S.K., Wold, M.S., and Burgers, P.M.J. (2006). Replication protein A directs loading of the DNA damage checkpoint clamp to 5′-DNA junctions. J. Biol. Chem. *281*, 27855–27861.

Mehta, A., and Haber, J.E. (2014). Sources of DNA double-strand breaks and models of recombinational DNA repair. Cold Spring Harb. Perspect. Biol. *6*, a016428.

Mimitou, E.P., and Symington, L.S. (2008). Sae2, Exo1 and Sgs1 collaborate in DNA double-strand break processing. Nature *455*, 770–774.

Mordes, D.A., Nam, E.A., and Cortez, D. (2008). Dpb11 activates the Mec1-Ddc2 complex. Proc. Natl. Acad. Sci. USA *105*, 18730–18734.

Myler, L.R., Gallardo, I.F., Soniat, M.M., Deshpande, R.A., Gonzalez, X.B., Kim, Y., Paull, T.T., and Finkelstein, I.J. (2017). Single-molecule imaging reveals how Mre11-Rad50-Nbs1 initiates DNA break repair. Mol. Cell *67*, 891–898.e4.

Navadgi-Patil, V.M., and Burgers, P.M. (2008). Yeast DNA replication protein Dpb11 activates the Mec1/ATR checkpoint kinase. J. Biol. Chem. *283*, 35853–35859.

Navadgi-Patil, V.M., and Burgers, P.M. (2009). The unstructured C-terminal tail of the 9-1-1 clamp subunit Ddc1 activates Mec1/ATR via two distinct mechanisms. Mol. Cell *36*, 743–753.

Ngo, G.H.P., and Lydall, D. (2015). The 9-1-1 checkpoint clamp coordinates resection at DNA double strand breaks. Nucleic Acids Res. *43*, 5017–5032.

Nguyen, A.T., and Zhang, Y. (2011). The diverse functions of Dot1 and H3K79 methylation. Genes Dev. *25*, 1345–1358.

Nicolette, M.L., Lee, K., Guo, Z., Rani, M., Chow, J.M., Lee, S.E., and Paull, T.T. (2010). Mre11-Rad50-Xrs2 and Sae2 promote 5′ strand resection of DNA double-strand breaks. Nat. Struct. Mol. Biol. *17*, 1478–1485.

Nimonkar, A.V., Genschel, J., Kinoshita, E., Polaczek, P., Campbell, J.L., Wyman, C., Modrich, P., and Kowalczykowski, S.C. (2011). BLM-DNA2-RPA-MRN and EXO1-BLM-RPA-MRN constitute two DNA end resection machineries for human DNA break repair. Genes Dev. *25*, 350–362.

Niu, H., Chung, W.H., Zhu, Z., Kwon, Y., Zhao, W., Chi, P., Prakash, R., Seong, C., Liu, D., Lu, L., et al. (2010). Mechanism of the ATP-dependent DNA end-resection machinery from *Saccharomyces cerevisiae*. Nature *467*, 108–111.

Pellicioli, A., Lee, S.E., Lucca, C., Foiani, M., and Haber, J.E. (2001). Regulation of *Saccharomyces* Rad53 checkpoint kinase during adaptation from DNA damage-induced G2/M arrest. Mol. Cell *7*, 293–300.

Pfander, B., and Diffley, J.F. (2011). Dpb11 coordinates Mec1 kinase activation with cell cycle-regulated Rad9 recruitment. EMBO J. *30*, 4897–4907.

Puddu, F., Granata, M., Di Nola, L., Balestrini, A., Piergiovanni, G., Lazzaro, F., Giannattasio, M., Plevani, P., and Muzi-Falconi, M. (2008). Phosphorylation of the budding yeast 9-1-1 complex is required for Dpb11 function in the full activation of the UV-induced DNA damage checkpoint. Mol. Cell. Biol. *28*, 4782–4793.

Reginato, G., Cannavo, E., and Cejka, P. (2017). Physiological protein blocks direct the Mre11-Rad50-Xrs2 and Sae2 nuclease complex to initiate DNA end resection. Genes Dev. *31*, 2325–2330.

Schwartz, M.F., Duong, J.K., Sun, Z., Morrow, J.S., Pradhan, D., and Stern, D.F. (2002). Rad9 phosphorylation sites couple Rad53 to the *Saccharomyces cerevisiae* DNA damage checkpoint. Mol. Cell *9*, 1055–1065.

Shibata, A., Moiani, D., Arvai, A.S., Perry, J., Harding, S.M., Genois, M.M., Maity, R., van Rossum-Fikkert, S., Kertokalio, A., Romoli, F., et al. (2014). DNA double-strand break repair pathway choice is directed by distinct MRE11 nuclease activities. Mol. Cell *53*, 7–18.

Shroff, R., Arbel-Eden, A., Pilch, D., Ira, G., Bonner, W.M., Petrini, J.H., Haber, J.E., and Lichten, M. (2004). Distribution and dynamics of chromatin modification induced by a defined DNA double-strand break. Curr. Biol. *14*, 1703–1711.

Sweeney, F.D., Yang, F., Chi, A., Shabanowitz, J., Hunt, D.F., and Durocher, D. (2005). *Saccharomyces cerevisiae* Rad9 acts as a Mec1 adaptor to allow Rad53 activation. Curr. Biol. *15*, 1364–1375.

Toh, G.W., O'Shaughnessy, A.M., Jimeno, S., Dobbie, I.M., Grenon, M., Maffini, S., O'Rorke, A., and Lowndes, N.F. (2006). Histone H2A phosphorylation and H3 methylation are required for a novel Rad9 DSB repair function following checkpoint activation. DNA Repair (Amst.) *5*, 693–703.

Villa, M., Cassani, C., Gobbini, E., Bonetti, D., and Longhese, M.P. (2016). Coupling end resection with the checkpoint response at DNA double-strand breaks. Cell. Mol. Life Sci. *73*, 3655–3663.

Wang, H., and Elledge, S.J. (2002). Genetic and physical interactions between DPB11 and DDC1 in the yeast DNA damage response pathway. Genetics *160*, 1295–1304.

Wang, W., Daley, J.M., Kwon, Y., Krasner, D.S., and Sung, P. (2017). Plasticity of the Mre11-Rad50-Xrs2-Sae2 nuclease ensemble in the processing of DNA-bound obstacles. Genes Dev. *31*, 2331–2336.

Westmoreland, J.W., and Resnick, M.A. (2016). Recombinational repair of radiation-induced double-strand breaks occurs in the absence of extensive resection. Nucleic Acids Res. *44*, 695–704.

Wysocki, R., Javaheri, A., Allard, S., Sha, F., Coté, J., and Kron, S.J. (2005). Role of Dot1-dependent histone H3 methylation in G1 and S phase DNA damage checkpoint functions of Rad9. Mol. Cell. Biol. *25*, 8430–8443.

Zakharyevich, K., Ma, Y., Tang, S., Hwang, P.Y., Boiteux, S., and Hunter, N. (2010). Temporally and biochemically distinct activities of Exo1 during meiosis: double-strand break resection and resolution of double Holliday junctions. Mol. Cell *40*, 1001–1015.

Zhu, Z., Chung, W.H., Shim, E.Y., Lee, S.E., and Ira, G. (2008). Sgs1 helicase and two nucleases Dna2 and Exo1 resect DNA double-strand break ends. Cell *134*, 981–994.

Zou, L., and Elledge, S.J. (2003). Sensing DNA damage through ATRIP recognition of RPA-ssDNA complexes. Science *300*, 1542–1548.

STAR★METHODS

KEY RESOURCES TABLE

REAGENT or RESOURCE	SOURCE	IDENTIFIER
Antibodies		
Anti-Rad53	Abcam	Ab104232; RRID: AB_2687603
Anti-HA (12CA5)	In house antibody	N/A
Bacterial and Virus Strains		
Subcloning Efficiency DH5alpha Competent Cells	Invitrogen	18265017
Chemicals, Peptides, and Recombinant Proteins		
SspI-HF	NEB	R3132L
SsoFast™ EvaGreen®Supermix, 500 Rxn	Bio-Rad	1725201
Hygromycin B	Roche	10843555001
ClonNAT (nourseothricin)	WERNERBioAgents	96736-11-7
G-418 disulfate	Medchemexpress	HY-17561
Phleomycin	Sigma-Aldrich	P9564-100MG
(S)-(+)-Camptothecin	Sigma-Aldrich	C9911-1G
Methyl methanesulfonate	Sigma-Aldrich	129925/25G
Trichloroacetic acid	Sigma-Aldrich	91230-1KG
RNase A	Roche	10109169001
Bromophenol Blue sodium salt	Sigma-Aldrich	B6131-25G
Phenylmethanesulfonyl fluoride	Sigma-Aldrich	78830-5G
tRNA	Roche	10109495001
Sodium chloride	Sigma-Aldrich	31434-1KG-R-D
Formamide	Sigma-Aldrich	47671-1L-F
Denhardt's Solution 50x	Sigma-Aldrich	D2532-5X5ML
Hydrochloric acid	Sigma-Aldrich	30721-1L-M
Yeast nitrogen base with amino acids	Sigma-Aldrich	Y1250-250G
Deoxyribonucleic acid, single stranded from salmon testes	Sigma-Aldrich	D7656-5X1ML
SSPE buffer 20X concentrate	Sigma-Aldrich	S2015-1L
Dimethyl sulfoxide	Sigma-Aldrich	D4540-1L
Triton® X-100 for molecular biology	Sigma-Aldrich	T8787-100ML
Ficoll® PM 400	Sigma-Aldrich	F4375-25G
Sodium deoxycholate	Sigma-Aldrich	30970-100G
Lithium chloride	Sigma-Aldrich	L9650-100G
Dextran sulfate sodium salt from leuconostoc. spp	Sigma-Aldrich	D8906-100G
N,N,N',N'-Tetramethylethylenediamine	Sigma-Aldrich	T9281-50ML
Acrilamide 4X solution	Serva	10677.1
N,N'-Methylene-bisacrylamide 2X	Serva	29197.01
IGEPAL® CA-630	Sigma-Aldrich	I8896-100ML
Ammonium persulfate	Sigma-Aldrich	A3678-25G
DL-Dithiothreitol	Sigma-Aldrich	43819-25G
HEPES	Sigma-Aldrich	H4034-1KG
Ethylenediaminetetraacetic acid $\geq$ 98.0%	Sigma-Aldrich	03620-1KG
Complete Mini	Roche	11836153001
Peroxide solution and Enhancer solution	Genespin	STS-E500
D-Sorbitol	Sigma-Aldrich	S7547-1KG
Ponceau s sodium practical grade	Sigma-Aldrich	P3504-100G

(*Continued on next page*)

Continued

REAGENT or RESOURCE	SOURCE	IDENTIFIER
Trizma® base	Sigma-Aldrich	33742-2KG
Sodium dodecyl sulfate	Sigma-Aldrich	L3771-500G
Sodium hydroxyde	Merck Millipore	1064621000
Formaldehyde solution for molecular biology, 36.5-38% in H2O	Sigma-Aldrich	F8775-500ML
Glycine for electrophoresis, ≥ 99%	Sigma-Aldrich	G8898-1KG
2-Propanol	Sigma-Aldrich	I9516-500ML
Ethanol absolute	Sigma-Aldrich	02860-2,5L
Zymolyase 20T	Nacalai Tesque	07663-91
EASYTIDES UTP [alpha-32P]	Perkin Elmer	NEG507T250UC
Dynabeads Protein G	Invitrogen	10004D
Agarose LE	Euroclone	EMR920500-500 g
D(+)-Raffinose pentahydrate	Sigma-Aldrich	83400-100G
D(+)-Galactose	Sigma-Aldrich	48260-500G-F
D-(+)-Glucose monohydrate	Sigma-Aldrich	49159-5KG
Yeast Extract Difco	BD	212750
Peptone Difco	BD	211677
Peptone Oxoid	OXOID	LP0037T
Yeast extract Oxoid	OXOID	LP0021T
Agar Bacto Difco	BD	214030
Agarose LE	EuroClone	EMR920500-500 g
Critical Commercial Assays		
DECA-prime II Random Primed DNA labeling Kit	Promega	P1440
QIAGEN QIAquick PCR Purification kit	QIAGEN	28106
Experimental Models: Organisms/Strains		
S. cerevisiae, see Table S1	This study	N/A
Oligonucleotides		
ARO+: TGAGTCGTTACAAGGTGATGCC	This study	N/A
ARO-: ACCTACAGGAGGACCCGAAA	This study	N/A
DSB 0.2+ TCAGACTCAAGCAAACAATCAA	This study	N/A
DSB 0.2-: CCCGTATAGCCAATTCGTTC	This study	N/A
DSB 0.6+: CACCCAAGAAGGCGAATAAG	This study	N/A
DSB 0.6-: CATGCGGTTCACATGACTTT	This study	N/A
DSB 1.8+: ACGTCGTTGTTAATGGTGGTG	This study	N/A
DSB 1.8-: CGCGAGTCTTATGCCAAAAA	This study	N/A
DSB 5.4 +: CGAGGAAAATGGTGGGATAA	This study	N/A
DSB 5.4 -: GGACGACTTTAAGATGGA AGGA	This study	N/A
Software and Algorithms		
Bio-Rad CFX Maestro	Bio-Rad	
Other		
White 48-well PCR plates Multiplate™	Bio-Rad	MLL4851
Nylon hybridization transfer membrane	GeneScreen	NEF1018001PK
Nitrocellulose blotting membrane, Amersham™ Protran™ 0.45 μm NC	GE Healthcare	10600002

RESOURCE AVAILABILITY

Lead contact

Further information and requests for resources and reagents should be directed to and will be fulfilled by the Lead Contact, Maria Pia Longhese (mariapia.longhese@unimib.it).

Materials availability
All unique/stable reagents generated in this study are available from the Lead Contact without restriction.

Data and code availability
This study did not generate any unique datasets or code.

EXPERIMENTAL MODEL AND SUBJECT DETAILS

Saccharomyces cerevisiae is the experimental model used in this study. Strain genotypes are listed in Table S1. Strain JKM139, used to detect DSB resection, was kindly provided by J. Haber (Brandeis University, Waltham, USA). Strain used to monitor Lys+ recombinants was kindly provided by S. Jinks-Robertson (Duke University School of Medicine, Durham, USA). The *ddc1-T602A* and *rad9-STAA* alleles were kindly provided by J. Diffley (The Francis Crick Institute, London UK) and B. Pfander (Max Planck Institute of Biochemistry, Martinsried, Germany). The JKM139 *mre11-H125N exo1Δ sgs1Δ* strain was kindly provided by G. Ira (Baylor College of Medicine, Houston, USA). The pRS316 *DDC2-RAD53-3FLAG* (*DDC2-RAD53*) plasmid was kindly provided by D. Stern (University of California, San Francisco). Gene disruptions were generated by one-step PCR homology cassette amplification and standard yeast transformation method.

METHOD DETAILS

Yeast media
Cells were grown in YEP medium (1% yeast extract, 2% bactopeptone) supplemented with 2% glucose (YEPD), 2% raffinose (YEPR) or 2% raffinose and 3% galactose (YEPRG). All the experiments have been performed at 27°C.

Search for suppressors of the DNA damage sensitivity of *exo1Δ sgs1Δ* cells
To search for suppressor mutations of the CPT-sensitivity of *exo1Δ sgs1Δ* cells, $5x10^6$ *exo1Δ sgs1Δ* cells were plated on YEPD in the presence of CPT or phleomycin. Survivors were crossed to wild-type cells to identify by tetrad analysis the suppression events that were due to single-gene mutations. Genomic DNA from two single-gene suppressors was analyzed by next-generation Illumina sequencing (IGA technology services) to identify mutations altering open reading frames within the reference *S. cerevisiae* genome. To confirm that the *rad24-E334** and *dpb11-L410F* alleles were responsible for the suppression, the *URA3* gene was integrated downstream of the *rad24-E334** and *dpb11-L410F* stop codon, and the resulting strain was crossed to wild-type cells to verify by tetrad dissection that the suppression of the *exo1Δ sgs1Δ* sensitivity co-segregated with the *URA3* allele.

Spot assays
Cells grown overnight were diluted to $1x10^7$ cells/ml. 10-fold serial dilutions were spotted on YEPD with or without indicated DNA damaging drugs. Plates were incubated for 3 days at 28°C.

Recombination assay
To measure recombination frequency, we used a strain carrying the *lys2::I-SceI* recipient allele at the *LYS2* locus on chromosome II containing an I-*Sce*I cleavage site, the *lys2* donor allele (*ly2Δ3′)* at the *CAN1* locus on chromosome V and a galactose-inducible I-*Sce*I gene inserted at the *HIS3* locus on chromosome XV (*his3Δ::kanMX-pGAL-I-SceI*) (Guo et al., 2017). I-*Sce*I expression was induced by adding galactose (1% final concentration) to cells growing exponentially in YEPR. Following galactose addition, cells were plated on YEPD and SC-lys media, incubated at 30°C and repair frequencies were calculated as the ratio of Lys^+ to total colonies. Data for each strain were based on at least three independent experiments, with 15 independent cultures per experiment.

DSB resection at the MAT locus
DSB end resection at the *MAT* locus in JKM139 derivative strains was analyzed on alkaline agarose gels, by using a single-stranded probe complementary to the unresected DSB strand, as previously described (Cassani et al., 2016). Quantitative analysis of DSB resection was performed by calculating the ratio of band intensities for ssDNA and total amount of DSB products.

Protein extract preparation and western blotting
Protein extracts for western blot analysis were prepared by trichloroacetic acid (TCA) precipitation. Frozen cell pellets were resuspended in 200 μL 20% TCA. After the addition of acid-washed glass beads, the samples were vortexed for 10 min. The beads were washed with 200 μL of 5% TCA twice, and the extract was collected in a new tube. The crude extract was precipitated by centrifugation at 3000 rpm for 10 min. TCA was discarded, and samples were resuspended in 70 μL 6X Laemmli buffer (60mM Tris, pH6.8, 2% SDS, 10% glycerol, 100mM DTT, 0.2% bromophenol blue) containing 0.9% B-mercaptoethanol and 30 μL 1M Tris (pH8.0). Prior to loading, samples were boiled at 95°C and centrifuged at 3.000 rpm for 10 min. Supernatant containing the solubilized proteins were separated on 10% polyacrylamide gels. Rad53 was detected by using anti-Rad53 polyclonal antibodies (ab104232) from Abcam.

Chromatin Immunoprecipitation and qPCR

ChIP analysis was performed as previously described (Cassani et al., 2016). Quantification of immunoprecipitated DNA was achieved by quantitative real-time PCR (qPCR) on a Bio-Rad MiniOpticon apparatus. Triplicate samples in 20 μL reaction mixture containing 10 ng of template DNA, 300 nM for each primer, 2 × SsoFast EvaGreen® supermix (Bio-Rad #1725201) (2 × reaction buffer with dNTPs, Sso7d-fusion polymerase, $MgCl_2$, EvaGreen dye, and stabilizers) were run in white 48-well PCR plates Multiplate (Bio-Rad #MLL4851). The qPCR program was as follows: step 1, 98°C for 2 min; step 2, 90°C for 5 s; step 3, 60°C for 15 s; step 4, return to step 2 and repeat 45 times. At the end of the cycling program, a melting program (from 65°C to 95°C with a 0.5°C increment every 5 s) was run to test the specificity of each qPCR. Data are expressed as fold enrichment at the HO-induced DSB over that at the non-cleaved *ARO1* locus, after normalization of each ChIP signals to the corresponding input for each time point. Fold enrichment was then normalized to the efficiency of DSB induction.

QUANTIFICATION AND STATISTICAL ANALYSIS

Data are expressed as mean values ± standard deviation. Quantification and statistical analysis were done using PRISM (GraphPad). *p* values for the ChIP-qPCR and recombination experiments were calculated by two-tailed Student's t test. No statistical methods or criteria were used to estimate sample size or to include or exclude samples.